ACS APPLIED MATERIALS & INTERFACES

Research Article

www.acsami.org

In-Situ-Reduced Synthesis of Ti^{3+} Self-Doped TiO_2/g-C_3N_4 Heterojunctions with High Photocatalytic Performance under LED Light Irradiation

Kai Li,[†] Shanmin Gao,*[,†,‡] Qingyao Wang,[†] Hui Xu,[†] Zeyan Wang,[‡] Baibiao Huang,*[,‡] Ying Dai,[‡] and Jun Lu*[,§]

[†]College of Chemistry and Materials Science, Ludong University, Yantai 264025, China

[‡]State Key Laboratory of Crystal Materials, Shandong University, Jinan 250100, China

[§]Chemical Sciences and Engineering Division, Argonne National Laboratory, Lemont, Illinois 60439, United States

ABSTRACT: A simple one-step calcination route was used to prepare Ti^{3+} self-doped TiO_2/g-C_3N_4 heterojunctions by mixture of $H_2Ti_3O_7$ and melamine. X-ray diffraction (XRD), transmission electron microscopy (TEM), high-resolution transmission electron microscopy (HRTEM), X-ray photoelectron spectroscopy (XPS), electron spin resonance (ESR) spectroscopy, and UV−Vis diffuse reflectance spectroscopy (UV−vis DRS) technologies were used to characterize the structure, crystallinity, morphology, and chemical state of the as-prepared samples. The absorption of the prepared Ti^{3+} self-doped TiO_2/g-C_3N_4 heterojunctions shifted to a longer wavelength region in comparison with pristine TiO_2 and g-C_3N_4. The photocatalytic activities of the heterojunctions were studied by degrading methylene blue under a 30 W visible-light-emitting diode irradiation source. The visible-light photocatalytic activities enhanced by the prepared Ti^{3+} self-doped TiO_2/g-C_3N_4 heterojunctions were observed and proved to be better than that of pure TiO_2 and g-C_3N_4. The photocatalysis mechanism was investigated and discussed. The intensive separation efficiency of photogenerated electron−hole in the prepared heterojunction was confirmed by photoluminescence (PL) spectra. The removal rate constant reached 0.038 min^{-1} for the 22.3 wt % Ti^{3+} self-doped TiO_2/g-C_3N_4 heterojunction, which was 26.76 and 7.6 times higher than that of pure TiO_2 and g-C_3N_4, respectively. The established heterojunction between the interfaces of TiO_2 nanoparticles and g-C_3N_4 nanosheets as well as introduced Ti^{3+} led to the rapid electron transfer rate and improved photoinduced electron−hole pair's separation efficiency, resulting in the improved photocatalytic performance of the Ti^{3+} self-doped TiO_2/g-C_3N_4 heterojunctions.

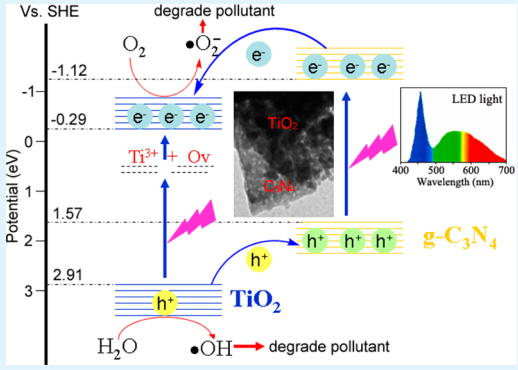

KEYWORDS: *Ti^{3+} self-doped, TiO_2/g-C_3N_4 heterojunctions, visible-light photocatalytic, LED light source*

1. INTRODUCTION

Among the semiconducting materials, TiO_2 is one of the most promising photocatalysts due to its excellent chemical resistance and nontoxicity. However, TiO_2 has its own drawbacks, especially the wide band gaps which lead to the low visible-light utilization and the high recombination rate of photoinduced holes and electrons. Therefore, the key factor in manufacturing highly active TiO_2 photocatalyst is to find a way to narrow the band gap and restrain the photoinduced electron−hole pair recombination.[1] Both metal/nonmetal doping and surface noble metal modification have been adopted to change the physical properties and electronic structures of TiO_2.[2,3] However, this type of conventional impurities doping or heterogeneous modification elements forms the impurity defect, which acts as the recombination center of photoinduced carriers and reduces the thermal stability, consequently leading to the lower photocatalytic performance.

Instead of adding impurities, recent work reported that the local states will be formed at the bottom of the comduction band (CB) of TiO_2 by only introducing Ti^{3+} or oxygen vacancies (O_V) into the lattice. Hence, such Ti^{3+} self-doped TiO_2 achieved its visible-light absorption performance while eliminating the recombination effect from doped impurities.[4] In addition, the electrical conductivity of TiO_2 can be increased and the transfer of photogenerated carriers can be accelerated through introduced Ti^{3+}.[5]

Another way to control the recombination of photoinduced electrons and holes is to recombine two different semiconductors with an appropriate energy band into the heterojunction structure. The heterojunctions can accelerate the separation of electron and hole, prolong charge life, and increase the efficiency of photocatalysis. Numbers of semi-

Received: December 3, 2014
Accepted: April 13, 2015
Published: April 13, 2015

DOI: 10.1021/am508505n
ACS Appl. Mater. Interfaces 2015, 7, 9023−9030

conductors are able to form heterojunctions with TiO_2 and improve the photocatalytic activity to certain degrees.[6,7] Recently, the graphitic C_3N_4 (g-C_3N_4) has attracted considerable attention, because it has narrow band gap (2.7 eV) and can be irradiated by visible light to exhibit excellent photocatalytic activity.[8−10] Such g-C_3N_4 can be prepared through bulk reaction or polycondensation via the pyrolysis of nitrogen-rich precursors, such as melamine, urea, cyanamide, and dicyandiamide.[11−13] However, the pure g-C_3N_4 has higher carrier recombination odds and a smaller surface area, leading to lower photocatalytic activity.[14,15] Compared with bulk g-C_3N_4, the g-C_3N_4 nanosheets have a larger surface area and shorter transferring distance of photoinduced charge carriers[16,17] but easily aggregate during one-step pyrolysis. In order to obtain the satisfied nanostructures, it usually requires either step-by-step heating or desquamating the bulk g-C_3N_4 in water through ultrasound for a long time.[17−19] In addition, many attempts have been implemented to improve the quantum efficiency of g-C_3N_4, such as coupling g-C_3N_4 with other semiconductors to improve the separation rate of the electron−hole pair. Various g-C_3N_4/semiconductor heterojunctions or composites photocatalysts, such as CdS,[20] WO_3,[21] ZnO,[22−24] tungstate (Bi_2WO_6, $ZnWO_4$),[25,26] and vanadate ($GdVO_4$, Ag_3VO_4, $SmVO_4$),[27−29] have been prepared for the photodegradation of pollutants.

The established heterostructure between g-C_3N_4 and TiO_2 is an effective way to improve the efficiency of charge separation in the photocatalyst system of g-C_3N_4/TiO_2 composites.[30−32] During the photocatalytic reaction using an UV irradiation source, the photoinduced holes jump from the valence band (VB) of TiO_2 to that of g-C_3N_4 while the electrons jump from the CB of g-C_3N_4 to that of TiO_2. However, only random electrons can be generated under visible-light irradiation because of the wide band gap of TiO_2, low electron transfer rate from g-C_3N_4 to TiO_2, and therefore high recombination of photoinduced carriers. In order to further improve the photocatalytic efficiency of the g-C_3N_4/TiO_2 composite under visible-light irradiation, N-, S-, or C-doped TiO_2/C_3N_4 composites have been investigated.[33,34]

The photocatalytic performance of the composite photocatalysts can be affected by the mixing method. At present, the main preparation methods for TiO_2/g-C_3N_4 composite materials are ball milling followed by further calcination, ultrasonic dispersion, and impregnation by using the prepared g-C_3N_4 and TiO_2 as precursors.[33,35] However, the combination of TiO_2 and g-C_3N_4 is not strong enough due to these mechanical mixing methods. In this study, a simple strategy was established for hybridization of g-C_3N_4 nanosheets with Ti^{3+} self-doped TiO_2 nanoparticles to improve the visible-light photocatalytic activity. The Ti^{3+} self-doped TiO_2/g-C_3N_4 heterojunctions were prepared by one-step heating $H_2Ti_3O_7$ nanotubes mixed with melamine. The strong bonding was formed during the thermal formation of TiO_2 nanoparticles and g-C_3N_4 nanosheets. Meanwhile, Ti^{3+} and oxygen vacancy were also formed. In addition, a low-energy consumption light-emitting diode (LED) with high-energy conversion and low-heat production was chose as a visible-light source. To the best of our knowledge, there is no report on the preparation of Ti^{3+} self-doped TiO_2 nanoparticles coupled with g-C_3N_4 nanosheets by using a LED light source in a photocatalytic system. In this paper, the structure, morphology, and optical property of the samples are characterized by XRD, XPS, TEM, and UV−vis. The formation mechanism is proposed according to those results. In addition, the photocatalysis activity is studied by degrading methylene blue (MB) under LED irradiation. The possible photocatalysis mechanism of Ti^{3+} self-doped TiO_2/g-C_3N_4 heterojunctions is also discussed.

2. EXPERIMENTAL SECTION

2.1. Preparation of Photocatalysts. All chemicals, such as melamine, NaOH, $AgNO_3$, EDTA-Na, commercial TiO_2, *p*-benzoquinone (BQ), ammonium oxalate (AO), *tert*-butanol (TBA), and terephthalic acid (TA), were reagent grade and obtained from Sinopharm Chemical Reagent Co., Ltd. (Shanghai, China) without purification. Double-distilled water was used in the whole experimental process.

The hydrothermal synthesis of titanate ($H_2Ti_3O_7$) nanotubes was according to the literature procedure.[36] Typically, 1.5 g of TiO_2 powder was added to 80 mL of 10 M NaOH aqueous solution while stirring. Then the mixture was heated at 180 °C for 48 h in a Teflon-lined autoclave. The obtained precipitates were washed with 0.1 M HCl solution and stirred overnight at room temperature. The purified precipitates were rinsed with water several times followed by centrifuging. The obtained powders were dried in a vacuum drying chamber at 60 °C for 12 h.

The Ti^{3+} self-doped TiO_2/g-C_3N_4 heterojunctions were prepared by one-step heating the mixture of the $H_2Ti_3O_7$ nanotubes and melamine. In a typical procedure, 1 g of obtained $H_2Ti_3O_7$ nanotubes and appropriate amounts of melamine were mixed in 100 mL of water followed by an ultrasonic treatment for 30 min at normal temperature. The mixture was stirred at room temperature for 4 h. The white solid was obtained through centrifugation and dried at 60 °C. Then this white precursor in an alumina crucible was annealed at 520 °C for 4 h in a muffle furnace. The final products were collected for use without further treatment. In order to study the role of g-C_3N_4 content on the photocatalytic activity of the Ti^{3+} self-doped TiO_2/g-C_3N_4 heterojunctions, samples with different amount of g-C_3N_4 were prepared under the same conditions. The products were named as TCN-*x*, where the *x* refers to the weight ratio of melamine to $H_2Ti_3O_7$ nanotubes. The color of the samples changed from grayish yellow to light green-yellow dependent on C_3N_4 contents.

For comparison, pure g-C_3N_4 was synthesized from the traditional pyrolysis method where melamine and pure TiO_2 were obtained from the traditional hydrolysis method of $TiCl_4$.

2.2. Characterization. Thermogravimetric (TGA) measurements were performed in STA409PC Simultaneous Thermal Analysis. A 20 mg amount of sample was placed in an alumina crucible, and corresponding TGA performances were recorded under linear heating at a heating rate of 10 °C/min until temperature reaches 800 °C in an open system. A Rigaku D/max-2500VPC model X-ray diffractometer was used to characterize the crystalline phases of the final products by using Ni-filtered Cu Kα radiation from 10° to 70° at a scanning rate of 0.02° s^{-1}. A JEOL-2100 model microscope was used to observe the morphologies of the products. A G Micro Tech ESCA 3000 model X-ray photoelectron spectrometer was used to characterize the chemical state of elements in the as-prepared samples at a pressure of $>1 \times 10^{-9}$ Torr. The monochromatic is Al Kα with a photon energy of 1486.6 eV. Electron spin resonance (ESR) measurements were carried out using a FA-200 spectrometer/X-bond. UV−vis diffuse reflection spectra (DRS) were recorded on a Shimadzu UV-2550 UV−vis spectrophotometer at normal temperature from 250 to 800 nm, in which fine $BaSO_4$ was used as the reflectance standard. A PerkinElmer LS 55 Fluorescence Spectrometer with pulsed xenon discharge lamps was used to measure the photoluminescence (PL) spectra at room temperature.

2.3. Photocatalytic Experiment. MB dyes were used as model organic pollutants to evaluate the photocatalytic performances of the as-prepared Ti^{3+} self-doped TiO_2/g-C_3N_4 heterojunctions. A 30 W LED light (Shandong Tianshi Optoelectronic Technology Co. Ltd., China) was used as the light source. During the degradation process, 40 mg of sample was added to 80 mL of MB aqueous solution (20 mg/L) in a customized quartz reactor. In order to reach the

DOI: 10.1021/am508505n
ACS Appl. Mater. Interfaces 2015, 7, 9023−9030

adsorption/desorption equilibrium between MB and the sample, the suspension was stirred in the dark for 30 min before photocatalytic reaction. During photocatalytic reaction, about 3 mL of MB solution was taken out and centrifuged to remove trace catalysts every 10 min. A Shimadzu UV-2550 model UV−vis spectrophotometer was used to measure the centrifuged solution absorbance from 200 to 800 nm. In the process of the photocatalytic reaction, no oxygen was bubbled into the reactor. For comparative purposes, the photocatalytic reactions were carried out with pure TiO_2 g-C_3N4 by using the same process. The decoloration efficiency (DE) was calculated using eq 1

$$\mathrm{DE} = \frac{C_0 - C_t}{C_0} \times 100\% \quad (1)$$

where C_0 and C_t are the absorbance of the original solution and the photodegraded solution after time t, respectively.

The active species capture experiments were employed to study the photocatalysis mechanism. At the beginning, 10.0 mM TBA ($^{\bullet}OH$ quencher), EDTA-Na_2 (h^+ quencher), $AgNO_3$ (e^- quencher), and BQ ($^{\bullet}O_2^-$ quencher) were added to the MB aqueous solution.[37,38] Then the remaining experimental processes were similar to that of photocatalysis.

3. RESULTS AND DISCUSSION

3.1. Characterization of the Samples. In order to confirm the g-C_3N_4 contents and their thermostability in the obtained composites, a TGA experiment was carried out in an open system at different temperatures from room temperature to 800 °C at a heating rate of 10 °C/min. Figure 1 shows the

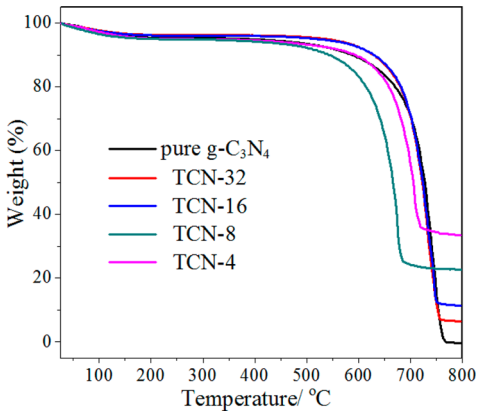

Figure 1. TGA curves for the pure g-C_3N_4 and Ti^{3+} self-doped TiO_2/g-C_3N_4 heterojunctions.

TG plots of different samples. From ambient temperature to 200 °C, little weight loss stages are observed. These weight losses are attributed to the desorption of the physically adsorbed and intercalated water. The main weight loss appears at the range of 500−760 °C due to the combustion of g-C_3N_4. The total weight loss is 100% for pure g-C_3N_4, which implies that it decomposes completely when the temperature reaches 750 °C. The second weight loss stage indicates the weight percent of g-C_3N_4 in the heterojunctions. The amount of g-C_3N_4 in the photocatalysts was measured to be 93.6, 88.8, 77.7, and 66.7 wt % for samples TCN-32, TCN-16, TCN-8, and TCN-4, respectively. In addition, the initial weight loss temperature for sample TCN-8 is lower than that of other samples, which is because the amount of TiO_2 is higher and g-C_3N_4 can be catalytically oxidized by the coupled TiO_2, even if at a heat treatment temperature lower than 600 °C.[27,29]

The XRD patterns of the pure g-C_3N_4 and the Ti^{3+} self-doped TiO_2/g-C_3N_4 heterojunctions are shown in Figure 2.

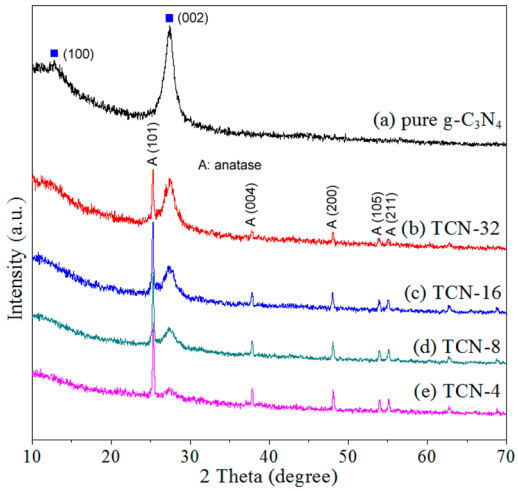

Figure 2. XRD patterns for the pure g-C_3N_4 (a) and Ti^{3+} self-doped TiO_2/g-C_3N_4 heterojunctions obtained at different melamine weight ratio. (b) TCN-32, (c) TCN-16, (d) TCN-8, and (e) TCN-4.

Two peaks are found in the pure g-C_3N_4, while the strongest one appeared at 27.38°, corresponding to an interlayer distance of 0.326 nm, indexed for the (002) plane of g-C_3N_4 (JCPDS, 87-1526),[15] and the small one at nearly 13.2° was indexed as the (100) plane of g-C_3N_4.[15] After in-situ chemical thermal decomposition of the $H_2Ti_3O_7$ and melamine mixture, strong diffraction peaks at 25.2°, 37.8°, 48.0°, 53.9°, 55.0°, and 62.4° were observed, corresponding to (101), (004), (200), (105), (211), and (204) crystal planes of anatase TiO_2 (JCPDS No. 21-1272), respectively. The relative diffraction intensity of g-C_3N_4 decreases gradually with increasing TiO_2 content.

TEM and HRTEM were used to observe the morphology of the obtianed samples. The pure g-C_3N_4 shows sheet-like structure, but there is serious aggregation (Figure 3a). From the decomposition of titanate, pure TiO_2 nanotubes are obtained that are about 9 nm in diameter and 150−350 nm in length (Figure 3b), which has no obvious difference from the $H_2Ti_3O_7$ nanotubes after heat treatment at 520 °C for 4 h (inset, Figure 3b). Figure 3c, 3d, and 3e shows that the heterojunctions of samples TCN-33, TCN-16, and TCN-8 are different from the pure TiO_2 or g-C_3N_4. In these TCN samples, the TiO_2 nanoparticles are attached to the nanosheets surface of g-C_3N_4 to form the heterojunction structures. The quantity of the TiO_2 nanoparticles increases with the decrease of the amount of melamine. Under HRTEM, the TCN-8 sample (Figure 3f) shows two different lattice fringes: one with d = 0.318 nm matches the (002) crystal interplanar of g-C_3N_4; the other one with d = 0.35 nm matches the (101) plane of anatase TiO_2. These results clearly prove that TiO_2 nanoparticles and g-C_3N_4 nanosheets are attached closely enough to form the heterojunctions, allowing the spatially smooth transformation of electron and hole between TiO_2 and g-C_3N_4. Moreover, no nanotube structure was observed in the heterojunction samples, indicating that the one-step thermal decomposition process of melamine to g-C_3N_4 affects the formation of TiO_2 dominantly, as discussed further below.

Figure 4 gives the high-resolution XPS spectra of C 1s, N 1s, O 1s, and Ti 2p in order to study the elemental valence state and surface composition of the obtained Ti^{3+} self-doped TiO_2/g-C_3N_4 heterojunctions. The fitting results from the experimental data for N 1s, O 1s, and Ti 2p of TCN-8 are also given. The peak at 284.7 eV is ascribed to surface adventitious carbon

DOI: 10.1021/am508505n
ACS Appl. Mater. Interfaces 2015, 7, 9023−9030

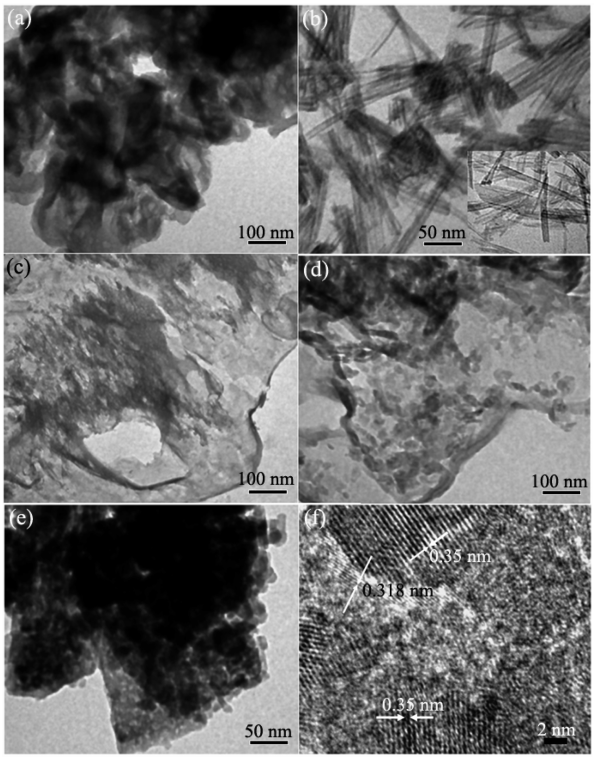

Figure 3. TEM and HRTEM images of (a) pure g-C_3N_4, (b) pure TiO_2 (the inset is $H_2Ti_3O_7$ image), (c) TCN-32, (d) TCN-16, and (e, f) TCN-8.

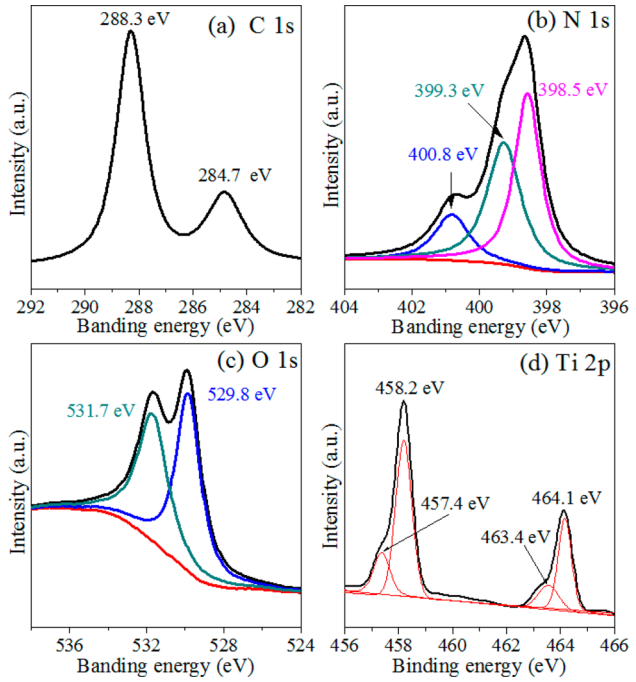

Figure 4. High-resolution XPS spectra of (a) C 1s, (b) N 1s, (c) O 1s, and (d) Ti 2p for sample TCN-8.

in the formation of the C−C bond, whereas the other peak at 288.3 eV corresponds to the sp^3-bonded C in N=C−N of g-C_3N_4 (Figure 4a).[39,40] Three peaks at 398.5, 399.3, and 400.8 eV deconvoluted from the N 1s peak belong to the pyridinic-like nitrogen (N−sp^2C), C−N−H, and N−$(C)_3$ bonding, respectively (Figure 4b).[41]

Two peaks with binding energies of 529.8 and 531.7 eV are observed in the high-resolution O 1s spectra (Figure 4c). The primary peak at 529.8 eV is attributed to the Ti−O band in TiO_2, and the secondary one at 531.7 eV is attributed to the surface −OH groups.[42] However, the peak of the oxygen in the TiO_2 lattice shifts to lower energy due to the existence of oxygen vacancy on the TiO_2 surface.[43] Such oxygen vacancy defects on the surface are able to trap the hole, promote the separation of electrons and holes, and thus reduce the recombination of the carriers.[43] In addition, hydroxyl radicals, $^{\bullet}$OH, with strong oxidation ability can be formed when the −OH group and adsorbed water trap the holes, which are capable of degrading the organic pollutants in water.[44] The binding energies of Ti $2p_{3/2}$ and Ti $2p_{1/2}$ of TCN-8 are located at 458.2 and 464.1 eV (Figure 4d), respectively, which are lower than those of pure TiO_2 (459.4 and 464.7 eV[45]).

In the fitting result of Ti $2p_{3/2}$ (Figure 4d), a major peak at 458.2 eV with a shoulder at 457.4 eV are ascribed to the $2p_{3/2}$ and $2p_{1/2}$ core levels of Ti^{3+}. Two peaks of 464.1 and 463.4 eV are assigned to the $2p_{3/2}$ and $2p_{1/2}$ core levels of Ti^{4+}. In order to satisfy the requirement of charge equilibrium, the Ov should be formed around Ti^{4+}; thus, the self-doped Ti^{3+} is formed in TiO_2.[46] As a defective state, Ti^{3+} can suppress the recombination of photoinduced electon−hole pairs and promote charge separation.[43]

ESR of samples TCN-4, TCN-8, and pure TiO_2 was carried out to investigate the uncoupled electrons and their interactions with the surrounding atoms, as shown in Figure 5. Both TCN-4

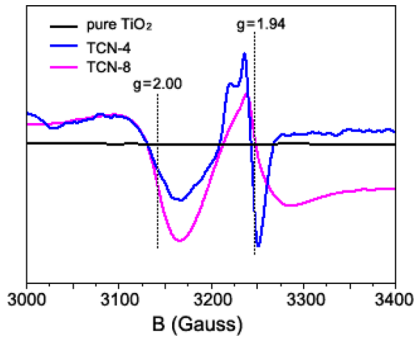

Figure 5. Electron spin resonance (ESR) spectra for samples TCN-4, TCN-8, and p-TiO_2.

and TCN-8 have a signal at about g = 1.94 corresponding to the Ti^{3+} signal peak.[4] However, an electron trapped on an O_V could only give a signal at g = 2.003 theoretically. Thus, the presence of surface Ti^{3+} is approved.[4] The ESR results also confirmed that Ti^{3+} not only existed in the lattice but also formed on the sample surface.

UV−vis diffuse reflection spectra are given in Figure 6. For comparison, the absorbance spectra of pure g-C_3N_4 and TiO_2 are also provided. The band gap of pure anatase TiO_2 is about 3.2 eV, so its absorption onset is located at about 388 nm, The pure g-C_3N_4 has a band gap of 2.71 eV, corresponding to the absorption onset of 458 nm.[8] In comparison with pure TiO_2 and g-C_3N_4, all heterojunction samples have stronger absorption in the visible range accompanying a red shift in the absorption edge, due to the synergistic effect between TiO_2 and g-C_3N_4 and the existence of Ti^{3+}.[38] These results indicated that the obtained heterojunctions could be stimulated by visible light, leading to more electrons and holes obtained. Therefore,

DOI: 10.1021/am508505n
ACS Appl. Mater. Interfaces 2015, 7, 9023−9030

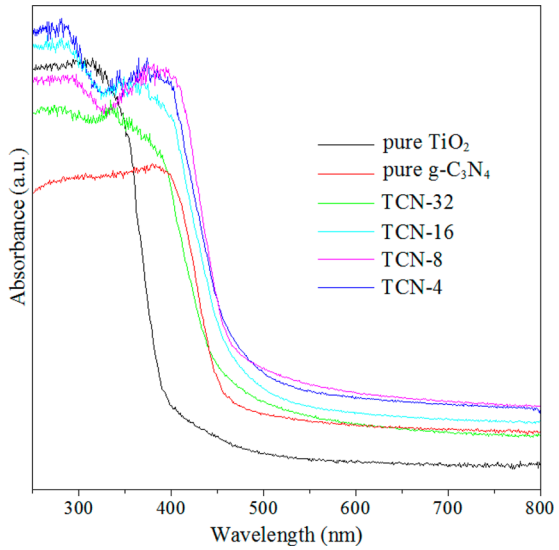

Figure 6. UV−vis spectra of pure g-C_3N_4, TiO_2, and Ti^{3+} self-doped TiO_2/g-C_3N_4 heterojunctions.

the heterojunctions should have favorable visible-light photocatalytic activity.

3.2. Formation Mechanism. After heat treatment, the melamine and $H_2Ti_3O_7$ nanotube will convert to g-C_3N_4 and TiO_2 nanotube or nanowire, respectively.[36] Since a one-step heating method usually leads to g-C_3N_4 aggregations, a step-by-step heat treatment is necessary to prepare flaky g-C_3N_4.[17] In addition, in order to break the $H_2Ti_3O_7$ nanotubes into small TiO_2 nanoparticles, the heating temperature needs to be higher than 600 °C.[47] In this study, the $H_2Ti_3O_7$ nanotubes and melamine are fully mixed as the raw material. After one-step heat treatment at 520 °C, the heterojunction composed by Ti^{3+} self-doped TiO_2 nanoparticles and g-C_3N_4 sheets was obtained. The possible formation mechanisms are shown in Figure 7. At

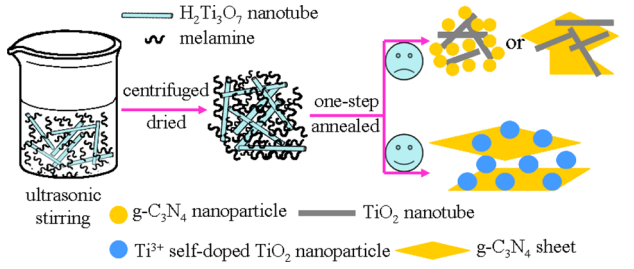

Figure 7. Formation mechanism of Ti^{3+} self-doped TiO_2/g-C_3N_4 heterojunctions.

the initial stage, the melamine was fully covered on the surface of $H_2Ti_3O_7$ nanotubes due to the formation of a hydrogen bond after ultrasonic treatment. Then it thermally decomposed into g-C_3N_4 and simultaneously released reducing gas such as NH_3 during the one-step thermal treatment.[48] At the same time, $H_2Ti_3O_7$ was decomposed and converted to TiO_2. Because of the well-dispersed melamine on the surface of $H_2Ti_3O_7$, the aggregation was restrained and the g-C_3N_4 sheets were obtained. Besides the $H_2Ti_3O_7$ nanotube self-collapse process, the reducing gas generated from the decomposition of melamine also can help it break into nanoparticles. Meanwhile, $H_2Ti_3O_7$ produced oxygen vacancies in such anoxic thermal decomposition condition, resulting in Ti^{3+} self-doped TiO_2.[47] Consequently, both Ti^{3+} and the oxygen vacancy defects can enhance the electronic conductivity and expand the light absorption range to the visible-light region.[4,47]

3.3. Photocatalytic Activity. Figure 8a provides the relationship between the wavelength and the intensity of the

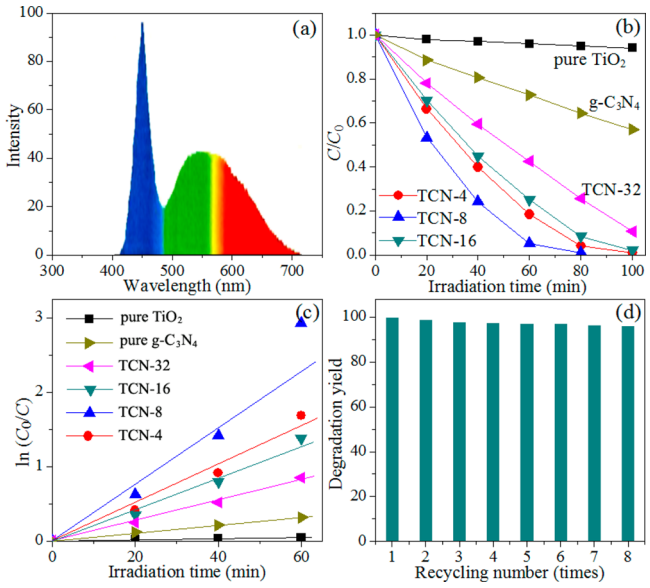

Figure 8. (a) Relation of the wavelength and intensity of the LED light source. (b) Photodegradation of MB solutions by using pure g-C_3N_4, TiO_2, and Ti^{3+} self-doped TiO_2/g-C_3N_4 heterojunctions as photocatalyst under LED light irradiation in neutral suspension. (c) Variation in the normalized $\ln(C_0/C)$ of the MB concentration as a function of irradiation time. (d) Recycling test of the sample TCN-8.

LED light source. It proves that the LED light source gives out visible light completely with the maximum wavelength coinciding with our samples. Figure 8b shows the photodegradation results of MB solutions with pure g-C_3N_4, TiO_2, or TCN-*x*. Under LED light illumination, all of the Ti^{3+} self-doped TiO_2/g-C_3N_4 heterojunctions samples have decent visible-light activity. In particular, TCN-8 shows its highest photodegradation ability on MB molecules, which are completely degraded within 80 min. In contrast, pure g-C_3N_4 exhibits limited activity, while pure TiO_2 shows relatively low visible-light activity. In addition, the photocatalytic activity of TCN-8 is better than that of individual Ti^{3+} self-doped TiO_2.[4]

Following the Langmuir−Hinshelwood model, the apparent reaction rate constants of the organic pollutants photocatalytic oxidation in aqueous suspensions can be obtained from eq 2[49]

$$\ln(C_0/C) = k_{app}t \quad (2)$$

where k_{app} is the pseudo-first-order rate constant, C_0 is the initial concentration of MB, and C is the MB concentration at reaction time t. From the linear time dependences of $\ln(C_0/C)$, the first-order rate constant k_{app} could be obtained. The greater the reaction rate constant, the better the photocatalytic activity. From Figure 8c, under LED irradiation, the sequence of the MB degradation rate constants is as follows TCN-8 > TCN-4 > TCN-16 > TCN-32 > pure g-C_3N_4 > pure TiO_2. Moreover, TCN-8 shows the highest value of first-order rate constant of k_{app} = 0.038 min^{-1}, which is about 26.76 and 7.6 times greater than that of pure TiO_2 and g-C_3N_4, respectively. It should be pointed out that since the photocatalytic reaction is a heterogeneous reaction and thus influenced by many factors,

DOI: 10.1021/am508505n
ACS Appl. Mater. Interfaces 2015, 7, 9023−9030

the degree of deviating from the first-order kinetics increased only for the samples with good photocatalytic properties.[49]

The stability of a photocatalyst is crucial for its practical application. Figure 8d shows the cyclic stability tests for sample TCN-8 under the same conditions. Apparently, there is no obvious decrease of its photocatalytic activity observed after 8 cycles, indicating that the strong combination of Ti^{3+} self-doped TiO_2 nanoparticles with g-C_3N_4 sheets successfully achieved high stability.

3.4. Enhanced Visible-Light Photocatalytic Activity Mechanism. The trapping, migration, and recombination of the charge carriers can be explored from the photoluminescence (PL) emission spectra of pure g-C_3N_4 and TCN-*x* samples excited by 320 nm UV light (Figure 9). The

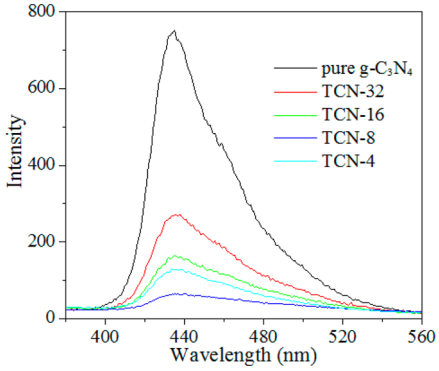

Figure 9. PL spectra of pure g-C_3N_4 and TCN-*x* samples under 320 nm excitation.

higher the peak intensity, the easier recombination of the photoinduced electrons and holes. For the pure g-C_3N_4 sample, the rapid recombination of the photoinduced electrons and holes leads to its low photocatalytic activity. Thus, its PL spectrum shows a strong emission from 400 to 550 nm at room temperature.[50] On the contrary, the quenching of PL intensity for the Ti^{3+} self-doped TiO_2/g-C_3N_4 heterojunctions indicated that the recombination of photoinduced electrons and holes of g-C_3N_4 can be suppressed by the presence of TiO_2. Moreover, the intensities decrease with the increased amount of TiO_2 until the g-C_3N_4 content drops to 66.7 wt %, which means that the photoactivity will decrease if there is a further decrease of g-C_3N_4.

In the photocatalytic process, the main oxidative species can be detected by adding 10.0 mM TBA ($^{\bullet}OH$ quencher), EDTA-Na_2 (h^+ quencher), $AgNO_3$ (e^- quencher), and BQ ($^{\bullet}O_2^-$ quencher) into the photocatalytic reaction systems. This is crucial for elucidating the photocatalytic mechanism. As shown in Figure 10, different scavengers have different effects on the degradation of MB over the TCN-8 heterojunction system. The addition of $^{\bullet}OH$ or h^+ quencher induces a small change in MB photodegradation. However, the photocatalytic activity of the TCN-8 heterojunction is greatly suppressed by addition of e^- or $^{\bullet}O_2^-$ quencher. Thus, $^{\bullet}O_2^-$ is the most critical specie, e^- is also important, and $^{\bullet}OH$ and h^+ are the least crucial ones during the MB photocatalytic process.

The above results confirmed that the synergistic effect of Ti^{3+} self-doped TiO_2 and g-C_3N_4 effectively improved the photocatalytic performance under LED light irradiation. It could be ascribed to several aspects: (1) the appropriate proportion of Ti^{3+} self-doped TiO_2 nanoparticles and g-C_3N_4 sheets helped form suitable TiO_2/g-C_3N_4 heterojunctions and sped up the

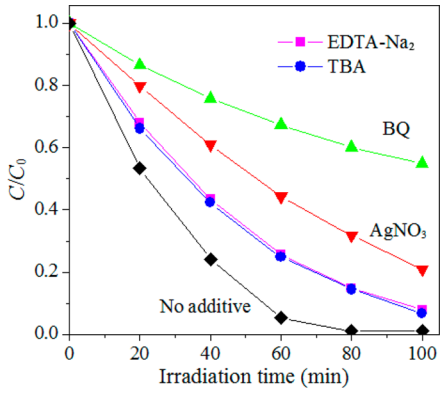

Figure 10. Photodegradation efficiency of MB on sample TCN-8 by adding the active species capture.

separation of charge carriers; (2) the existence of Ti^{3+} and Ov accelerated the electron transfer rate and suppressed the electron−hole pair recombination; (3) the g-C_3N_4 sheets increased the contact surface with TiO_2 nanoparticles, facilitated the transportation of reactants and products on photocatalyst surfaces, and resulted in easier chemical reactions; and (4) the g-C_3N_4 sheets can also shorten the photoinduced charger carrier transferring distance. The schematics of the electrochemical potentials of Ti^{3+} self-doped TiO_2 and g-C_3N_4 as well as the possible charge separation process of the heterojunctions are illustrated in Figure 11.

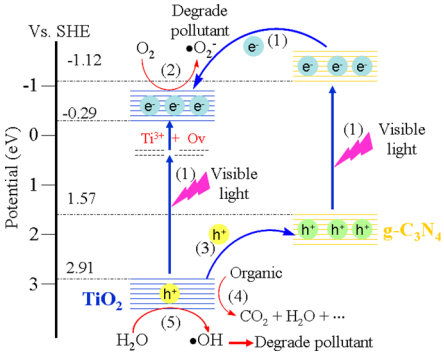

Figure 11. Schematic of the energy band of TiO_2 and g-C_3N_4 as well as charge migration and separation on Ti^{3+} self-doped TiO_2/g-C_3N_4 heterojunctions caused by LED light irradiation.

According to the CB and VB edge potentials of g-C_3N_4 and TiO_2 (−1.12 and 1.57 eV, −0.29 and 2.91 eV, respectively),[8] in the TiO_2/g-C_3N_4 heterojunctions, g-C_3N_4 could easily absorb the visible light because of its band gap (2.7 eV) . Once irradiated under a LED light source, the electrons are able to jump from the VB to the CB of g-C_3N_4 and then transfer from the CB of g-C_3N_4 to that of TiO_2. Such electron transition between heterojunctions can reduce the recombination of charge carriers and prolong the charge lifetime (Figure 11(1)).[51,52] In addition, the Ti^{3+} and Ov form a local state at the bottom of the TiO_2 CB with visible-light response capacity. Under visible-light irradiation, the electrons in the VB can jump to the CB of TiO_2 (Figure 11(1)). Then these excited-state electrons transfer to the TiO_2 nanoparticles surface to generate the main active groups of superoxide anion radicals ($^{\bullet}O_2^-$) through reacting with dissolved oxygen (Figure 11(2)), which further oxidize the MB. This is consistent with the test results

DOI: 10.1021/am508505n
ACS Appl. Mater. Interfaces 2015, 7, 9023−9030

of the main oxidative species (Figure 10). In addition, since the VB edge potential of TiO_2 is more positive than that of g-C_3N_4, the holes at the VB of TiO_2 can transfer to the VB of g-C_3N_4(Figure 11(3)). Because the standard redox potential of $^{\bullet}OH/OH^-$ is 1.99 V, the holes in C_3N_4 VB cannot induce $^{\bullet}OH$ from hydroxide or H_2O. However, the untransferred holes at the VB of TiO_2 sheets could directly oxidize the organic molecules (Figure 11(4)) and simultaneously react with H_2O to produce $^{\bullet}OH$ radical (Figure 11(5)). Since most of the holes in the VB of TiO_2 are transferred to the VB of C_3N_4, the number of holes in the VB of TiO_2 are significantly reduced; therefore, $^{\bullet}OH$ and h^+ are the least crucial active species during the MB photocatalytic process (Figure 10).

4. CONCLUSION

Ti^{3+} self-doped TiO_2 nanoparticles/g-C_3N_4 nanosheets heterojunctions were synthesized through one-step calcination of the $H_2Ti_3O_7$ nanotubes and melamine. Under this well-designed synthetic condition, the aggregation of g-C_3N_4 can be restrained and the formation of Ti^{3+} is promoted. The Ti^{3+} and Ov defects enhanced electronic conductivity and expanded the light absorption range to the visible-light region. The lifetime of electron−holes pairs was increased, and the recombination of the photogenerated charge carriers was reduced because of the heterojunctions at the interface between TiO_2 nanoparticles and g-C_3N_4 nanosheets. Such heterojunctions also efficiently reduced the recombination of photoinduced electron−hole pairs and increased the lifetime of charge carriers. Under visible LED light irradiation, the photocatalytic activities of the Ti^{3+} self-doped TiO_2/g-C_3N_4 heterojunctions were enhanced remarkably. This method provides a pathway to prepare the Ti^{3+} self-doped TiO_2/g-C_3N_4 heterojunctions for environmental purification of organic pollutants.

AUTHOR INFORMATION

Corresponding Authors

*E-mail: gaosm@ustc.edu.
*E-mail: bbhuang@sdu.edu.cn.
*E-mail: junlu@anl.gov.

Notes

The authors declare no competing financial interest.

ACKNOWLEDGMENTS

This work was supported by the Key Project of Natural Science Foundation of Shandong Province (ZR2013EMZ001), the National Basic Research Program of China (Grant No. 2013CB632401), the National Nature Science Foundation of China (51402145), and the Project of Shandong Province Higher Educational Science and Technology Program (J12LA01). This research has also been partially supported by the Program for Scientific Research Innovation Team in Colleges and Universities of Shandong Province. This work was also supported by the U.S. Department of Energy under Contract DE-AC0206CH11357 with the main support provided by the Vehicle Technologies Office, Department of Energy (DOE) Office of Energy Efficiency and Renewable Energy (EERE).

REFERENCES

(1) Ma, Y.; Wang, X. L.; Jia, Y. S.; Chen, X. B.; Han, H. X.; Li, L. Titanium Dioxide-Based Nanomaterials for Photocatalytic Fuel Generations. *Chem. Rev.* **2014**, *114*, 9987−10043.

(2) Chen, X. B.; Burda, C. The Electronic Origin of the Visible-Light Absorption Properties of C-, N- and S-Doped TiO_2 Nanomaterials. *J. Am. Chem. Soc.* **2008**, *130*, 5018−5019.

(3) Sun, L.; Zhai, J. L.; Li, H. Y.; Zhao, Y.; Yang, H. J.; Yu, H. W. Study of Homologous Elements: Fe, Co, and Ni Dopant Effects on the Photoreactivity of TiO_2 Nanosheets. *ChemCatChem* **2014**, *6*, 339−347.

(4) Liu, X.; Grabstanowicz, L. R.; Gao, S. M.; Xu, H.; Lou, Z. Z.; Wang, W. J.; Huang, B. B.; Dai, Y.; Xu, T. Green Synthetic Approach for Ti^{3+} Self-Doped TiO_{2-x} Nanoparticles with Efficient Visible Light Photocatalytic Activity. *Nanoscale* **2013**, *5*, 1870−1875.

(5) Wan, Z.; Huang, G. F.; Huang, W. Q.; Jiao, C.; Yan, X. G.; Yang, Z. M.; Zhang, Q. L. The Enhanced Photocatalytic Activity of Ti^{3+} Self-Doped TiO_2 by a Reduction Method. *Mater. Lett.* **2014**, *122*, 33−36.

(6) Yang, H. H.; Kershaw, S. V.; Wang, Y.; Gong, X. Z.; Kalytchuk, S.; Rogach, A. L.; Teoh, W. Y. Shuttling Photoelectrochemical Electron Transport in Tricomponent CdS/rGO/TiO_2 Nanocomposites. *J. Phys. Chem. C* **2013**, *117*, 20406−20414.

(7) Yang, J.; Wang, X. H.; Dai, J.; Li, J. T. Efficient Visible-Light-Driven Photocatalytic Dedgradation with Bi_2O_3 Coupling Silica Doped TiO_2. *Ind. Eng. Chem. Res.* **2014**, *53*, 12575−12586.

(8) Wang, X. C.; Maeda, K.; Thomas, A.; Takanabe, K.; Xin, G.; Carlsson, J. M.; Domen, K.; Antonietti, M. A Metal-Free Polymeric Photocatalyst for Hydrogen Production from Water under Visible Light. *Nat. Mater.* **2009**, *8*, 76−80.

(9) Zhang, J. S.; Chen, X. F.; Takanabe, K.; Maeda, K.; Domen, K.; Epping, J. D.; Fu, X. Z.; Antonietti, M.; Wang, X. C. Synthesis of a Carbon Nitride Structure for Visible-Light Catalysis by Copolymerization. *Angew. Chem., Int. Ed.* **2010**, *49*, 441−444.

(10) Jin, X.; Balasubramanian, V. V.; Selvan, S. T.; Sawant, D. P.; Chari, M. A.; Lu, G. Q.; Vinu, A. Highly Ordered Mesoporous Carbon Nitride Nanoparticles with High Nitrogen Content: A Metal-Free Basic Catalyst. *Angew. Chem., Int. Ed.* **2009**, *48*, 7884−7887.

(11) Dong, F.; Wang, Z. Y.; Sun, Y. J.; Ho, W. K.; Zhang, H. D. Engineering the Nanoarchitecture and Texture of Polymeric Carbon Nitride Semiconductor for Enhanced Visible Light Photocatalytic Activity. *J. Colloid Interface Sci.* **2013**, *401*, 70−79.

(12) Zhang, M.; Xu, J.; Zong, R. L.; Zhu, Y. F. Enhancement of Visible Light Photocatalytic Activities Via Porous Structure of g-C_3N_4. *Appl. Catal., B* **2014**, *147*, 229−235.

(13) Shiraishi, Y.; Kanazawa, S.; Sugano, Y.; Tsukamoto, D.; Sakamoto, H.; Ichikawa, S.; Hirai, T. Highly Selective Production of Hydrogen Peroxide on Graphitic Carbon Nitride (g-C_3N_4) Photocatalyst Activated by Visible Light. *ACS Catal.* **2014**, *4*, 774−780.

(14) Wang, X. C.; Blechert, S.; Antonietti, M. Polymeric Graphitic Carbon Nitride for Heterogeneous Photocatalysis. *ACS Catal.* **2012**, *2*, 1596−1606.

(15) Yan, S. C.; Li, Z. S.; Zou, Z. G. Photodegradation Performance of g-C_3N_4 Fabricated by Directly Heating Melamine. *Langmuir* **2009**, *25*, 10397−10401.

(16) Schwinghammer, K.; Mesch, M. B.; Duppel, V.; Ziegler, C.; Senker, J.; Lotsch, B. V. Crystalline Carbon Nitride Nanosheets for Improved Visible-Light Hydrogen Evolution. *J. Am. Chem. Soc.* **2014**, *136*, 1730−1733.

(17) Niu, P.; Zhang, L. L.; Liu, G.; Cheng, H. M. Graphene-Like Carbon Nitride Nanosheets for Improved Photocatalytic Activities. *Adv. Funct. Mater.* **2012**, *22*, 4763−4770.

(18) Cheng, N. Y.; Tian, J. Q.; Liu, Q.; Ge, C. J.; Qusti, A. H.; Asiri, A. M.; Al-Youbi, A. O.; Sun, X. P. Au-Nanoparticle-Loaded Graphitic Carbon Nitride Nanosheets: Green Photocatalytic Synthesis and Application Toward the Degradation of Organic Pollutants. *ACS Appl. Mater. Interfaces* **2013**, *5*, 6815−6819.

(19) Dong, F.; Ou, M. Y.; Jiang, Y. K.; Guo, S.; Wu, Z. B. Efficient and Durable Visible Light Photocatalytic Performance of Porous

DOI: 10.1021/am508505n
ACS Appl. Mater. Interfaces 2015, 7, 9023−9030

Carbon Nitride Nanosheets for Air Purification. *Ind. Eng. Chem. Res.* **2014**, *53*, 2318−2330.
(20) Zhang, J. Y.; Wang, Y. H.; Jin, J.; Zhang, J.; Lin, Z.; Huang, F.; Yu, J. G. Efficient Visible-Light Photocatalytic Hydrogen Evolution and Enhanced Photostability of Core/Shell CdS/g-C_3N_4 Nanowires. *ACS Appl. Mater. Interfaces* **2013**, *5*, 10317−10324.
(21) Katsumata, K.; Motoyoshi, R.; Matsushita, N.; Okada, K. Preparation of Graphitic Carbon Nitride (g-C_3N_4)/WO_3 Composites and Enhanced Visible-Light-Driven Photodegradation of Acetaldehyde Gas. *J. Hazard. Mater.* **2013**, *260*, 475−482.
(22) Sun, J. X.; Yuan, Y. P.; Qiu, L. G.; Jiang, X.; Xie, A. J.; Shen, Y. H.; Zhu, J. F. Fabrication of Composite Photocatalyst g-C_3N_4−ZnO and Enhancement of Photocatalytic Activity Under Visible Light. *Dalton Trans.* **2012**, *41*, 6756−6763.
(23) Chen, D. M.; Wang, K. W.; Xiang, D. G.; Zong, R. L.; Yao, W. Q.; Zhu, Y. F. Significantly Enhancement of Photocatalytic Performances Via Core−Shell Structure of ZnO@mpg-C_3N_4. *Appl. Catal., B* **2014**, *147*, 554−561.
(24) Zhu, Y. P.; Li, M.; Liu, Y. L.; Ren, T. Z.; Yuan, Z. Y. Carbon-doped ZnO Hybridized Homogeneously with Graphitic Carbon Nitride Nanocomposites for Photocatalysis. *J. Phys. Chem. C* **2014**, *118*, 10963−10971.
(25) Ge, L.; Han, C. C.; Liu, J. Novel Visible Light-Induced g-C_3N_4/Bi_2WO_6 Composite Photocatalysts for Efficient Degradation of Methyl Orange. *Appl. Catal., B* **2011**, *108−109*, 100−107.
(26) Sun, L. M.; Zhao, X.; Jia, C. J.; Zhou, Y. X.; Cheng, X. F.; Li, P.; Liu, L.; Fan, W. L. Enhanced Visible-Light Photocatalytic Activity of g-C_3N_4−$ZnWO_4$ by Fabricating a Heterojunction: Investigation Based on Experimental and Theoretical Studies. *J. Mater. Chem.* **2012**, *22*, 23428−23438.
(27) He, Y. M.; Cai, J.; Li, T. T.; Wu, Y.; Lin, H. J.; Zhao, L. L.; Luo, M. F. Efficient Degradation of RhB over $GdVO_4$/g-C_3N_4 Composites under Visible-Light Irradiation. *Chem. Eng. J.* **2013**, *215−216*, 721−730.
(28) Wang, S. M.; Li, D. L.; Sun, C.; Yang, S. G.; Guan, Y.; He, H. Synthesis and Characterization of g-C_3N_4/Ag_3VO_4 Composites with Significantly Enhanced Visible-Light Photocatalytic Activity for Triphenylmethane Dye Degradation. *Appl. Catal., B* **2014**, *144*, 885−892.
(29) Li, T. T.; Zhao, L. H.; He, Y. M.; Cai, J.; Luo, M. F.; Lin, J. J. Synthesis of g-C_3N_4/$SmVO_4$ Composite Photocatalyst with Improved Visible Light Photocatalytic Activities in RhB Degradation. *Appl. Catal., B* **2013**, *129*, 255−263.
(30) Gu, L. A.; Wang, J. Y.; Zou, Z. J.; Han, X. J. Graphitic-C_3N_4-Hybridized TiO_2 Nanosheets with Reactive {001} Facets to Enhance the UV- and Visible-Light Photocatalytic Activity. *J. Hazard. Mater.* **2014**, *268*, 216−223.
(31) Sridharan, K.; Jang, E.; Park, T. J. Novel Visible Light Active Graphitic C_3N_4-TiO_2 Composite Photocatalyst: Synergistic Synthesis, Growth and Photocatalytic Treatment of Hazardous Pollutants. *Appl. Catal., B* **2013**, *142*, 718−728.
(32) Miranda, C.; Mansilla, H.; Yánez, J.; Obregón, S.; Colón, G. Improved Photocatalytic Activity of g-C_3N_4/TiO_2 Composites Prepared by a Simple Impregnation Method. *J. Photochem. Photobiol. A: Chem.* **2013**, *253*, 16−21.
(33) Yang, N.; Li, G. Q.; Wang, W. L.; Yang, X. L.; Zhang, W. F. Photophysical and Enhanced Daylight Photocatalytic Properties of N-doped TiO_2/g-C_3N_4 Composites. *J. Phys. Chem. Solids* **2011**, *72*, 1319−1324.
(34) Kondo, K.; Murakami, N.; Ye, C.; Tsubota, T.; Ohno, T. Development of Highly Efficient Sulfur-Doped TiO_2 Photocatalysts Hybridized with Graphitic Carbon Nitride. *Appl. Catal., B* **2013**, *142−143*, 362−367.
(35) Pan, C. S.; Xu, J.; Wang, Y. J.; Li, D.; Zhu, Y. F. Dramatic Activity of C_3N_4/$BiPO_4$ Photocatalyst with Core/Shell Structure Formed by Self-Assembly. *Adv. Funct. Mater.* **2012**, *22*, 1518−1524.
(36) Kiatkittipong, K.; Ye, C. H.; Scott, J.; Amal, R. Understanding Hydrothermal Titanate Nanoribbon Formation. *Cryst. Growth Des.* **2010**, *10*, 3618−3625.
(37) Yang, X. F.; Cui, H. Y.; Li, Y.; Qin, J. L.; Zhang, R. X.; Tang, H. Fabrication of Ag_3PO_4-Graphene Composites with Highly Efficient and Stable Visible Light Photocatalytic Performance. *ACS Catal.* **2013**, *3*, 363−369.
(38) Wang, X. J.; Yang, W. Y.; Li, F. T.; Xue, Y. B.; Liu, R. H.; Hao, Y. J. In Situ Microwave-Assisted Synthesis of Porous N-TiO_2/g-C_3N_4 Heterojunctions with Enhanced Visible-Light Photocatalytic Properties. *Ind. Eng. Chem. Res.* **2013**, *52*, 17140−17150.
(39) Wang, X. C.; Chen, X. F.; Thomas, A.; Fu, X. Z.; Antonietti, M. Metal-Containing Carbon Nitride Compounds: a new Functional Organic−Metal Hybrid Material. *Adv. Mater.* **2009**, *21*, 1609−1612.
(40) Yan, H. J.; Chen, Y.; Xu, S. M. Synthesis of Graphitic Carbon Nitride by Directly Heating Sulfuric Acid Treated Melamine for Enhanced Photocatalytic H_2 Production from Water under Visible Light. *Int. J. Hydrogen Energy* **2012**, *37*, 125−133.
(41) Li, Y.; Zhang, H.; Liu, P.; Wang, D.; Li, Y.; Zhao, H. Cross-Linked g-C_3N_4/rGO Nanocomposites with Tunable Band Structure and Enhanced Visible Light Photocatalytic Activity. *Small* **2013**, *9*, 3336−3344.
(42) Zou, J.; Gao, J. C.; Wang, Y. Synthesis of Highly Active H_2O_2-Sensitized Sulfated Titania Nanoparticles with a Response to Visible Light, *J. Photochem. Photobiol. A* **2009**, *202*, 128−135.
(43) Szczepankiewicz, S. H.; Moss, J. A.; Hoffmann, M. R. Slow Surface Charge Trapping Kinetics on Irradiated TiO_2. *J. Phys. Chem. B* **2002**, *106*, 2922−2927.
(44) Liu, G.; Yan, X. X.; Chen, Z. G.; Wang, X. W.; Wang, L. Z.; Lu, G. Q.; Cheng, H. M. Synthesis of Rutile−Anatase Core−Shell Structured TiO_2 for Photocatalysis. *J. Mater. Chem.* **2009**, *19*, 6590−6596.
(45) Saha, N. C.; Tompkins, H. G. Titanium Nitride Oxidation Chemistry: An X-ray Photoelectron Spectroscopy Study. *J. Appl. Phys.* **1992**, *72*, 3072−3079.
(46) Su, J.; Zou, X. X.; Zou, Y. C.; Li, G. D.; Wang, P. P.; Chen, J. S. Porous Titania with Heavily Self-Doped Ti^{3+} for Specific Sensing of CO at Room Temperature. *Inorg. Chem.* **2013**, *52*, 5924−5930.
(47) Vittadini, A.; Schirmer, M.; Walz, M.-M.; Vollnhals, F.; Lukasczyk, T.; Steinruck, H.-P.; Marbach, H.; Riss, A.; Elser, M. J.; Schurer, B.; Diwald, O. Defects in Oxygen-Depleted Titanate Nanostructures. *Langmuir* **2012**, *28*, 7851−7858.
(48) Li, X. F.; Zhang, J.; Shen, L. H.; Ma, Y. M.; Cui, Q. L.; Zou, G. T. Preparation and Characterization of Graphitic Carbon Nitride Through Pyrolysis of Melamine. *Appl. Phys. A: Mater. Sci. Process.* **2009**, *94*, 387−392.
(49) Yu, J. G.; Wang, G. H.; Cheng, B.; Zhou, M. H. Effects of Hydrothermal Temperature and Time on the Photocatalytic Activity and Microstructures of Bimodal Mesoporous TiO_2 Powders. *Appl. Catal., B* **2007**, *69*, 171−180.
(50) Li, F. B.; Li, X. Z. Photocatalytic Properties of Gold/Gold Ion-Modified Titanium Dioxide for Wastewater Treatment. *Appl. Catal., A* **2002**, *228*, 15−27.
(51) Zhou, X. S.; Jin, B.; Li, L. D.; Peng, F.; Wang, H. J.; Yu, H.; Fang, Y. P. A Carbon Nitride/TiO_2 Nanotube Array Heterojunction Visible-Light Photocatalyst: Synthesis, Characterization, and Photoelectrochemical Properties. *J. Mater. Chem.* **2012**, *22*, 17900−179055.
(52) Choi, S. K.; Kim, S.; Lim, S. K.; Park, H. Photocatalytic Comparison of TiO_2 Nanoparticles and Electrospun TiO_2 Nanofibers: Effects of Mesoporosity and Interparticle Charge Transfer. *J. Phys. Chem. C* **2010**, *114*, 16475−16480.

DOI: 10.1021/am508505n
ACS Appl. Mater. Interfaces 2015, 7, 9023−9030